Mechanistic Modeling of Central Nervous System Pharmacokinetics and Target Engagement of HER2 Tyrosine Kinase Inhibitors to Inform Treatment of Breast Cancer Brain Metastases

Jing Li[1], Jun Jiang[1], Xun Bao[1], Vineet Kumar[2], Stephen C. Alley[2], Scott Peterson[3], and Anthony J. Lee[2]

ABSTRACT

Purpose: This study evaluated the central nervous system (CNS) pharmacokinetics and target engagement of lapatinib, neratinib, and tucatinib in patients with cancer, using a physiologically based pharmacokinetic (PBPK) modeling approach.

Experimental Design: Drug-specific parameters for *in vitro* metabolism, binding to plasma proteins and brain tissues, transcellular passive permeability, and interactions with efflux transporters were determined. Whole-body PBPK models integrated with a 4-compartment permeability-limited brain model was developed and verified for predicting plasma and CNS pharmacokinetics. Target engagement ratio (TER), defined as the ratio of the average steady-state unbound drug brain concentration ($C_{ss,ave,br}$) to *in vitro* IC_{50} for HER2 inhibition, was used as a predictor of intracranial efficacy.

Results: PBPK models predicted that following 1 cycle of standard dosing, tucatinib and lapatinib achieved similar $C_{ss,ave,br}$ (14.5 vs. 16.8 nmol/L), while neratinib $C_{ss,ave,br}$ (0.68 nmol/L) was 20-fold lower. Tucatinib and neratinib were equally potent for HER2 inhibition (IC_{50}, 6.9 vs. 5.6 nmol/L), while lapatinib was less potent (IC_{50}, 109 nmol/L). The model-predicted population mean TER in the human normal brain was 2.1 for tucatinib, but < 0.20 for lapatinib and neratinib.

Conclusions: The PBPK modeling suggests that tucatinib induces sufficient HER2 inhibition (TER > 2.0) in not only brain metastases with a disrupted blood–brain barrier (BBB), but also micrometastases where the BBB largely remains intact. These findings, in line with available clinical pharmacokinetics and efficacy data, support the therapeutic value of tucatinib for treatment of brain metastases and warrant further clinical investigation for the prevention of brain metastases in patients with HER2-positive breast cancer.

Introduction

Human epidermal growth factor receptor 2 (HER2), also known as erythroblastic leukemia viral oncogene homolog 2 (ERBB2) protein, is overexpressed in around 15%–20% of patients with breast cancer (1). HER2-positive breast cancer is associated with frequent and early brain metastases, with up to 50% of patients developing brain metastases during the course of their disease, and patients with brain metastasis have a poorer prognosis (2, 3). HER2-targeted therapies, including humanized monoclonal anti-HER2 antibodies (trastuzumab and pertuzumab), antibody–drug conjugates (trastuzumab emtansine and trastuzumab deruxtecan), and small-molecule tyrosine kinase inhibitors (lapatinib, neratinib, and tucatinib) targeting ERBB family receptors, have demonstrated survival benefit in patients with metastatic HER2-positive breast cancer (2). Nevertheless, effective systemic therapy for patients with brain metastases remains limited and represents a major clinical challenge.

Insufficient penetration of potentially effective therapeutic agents across the human blood–brain barrier (BBB) is a significant hurdle to efficacious treatment of primary and metastatic brain cancer. Compared to antibody-based anti-HER2 agents that do not readily penetrate the BBB (4), small-molecule HER2 tyrosine kinase inhibitors may have better BBB penetration and thus better intracranial activity. They have been extensively evaluated, as a single-agent or in combination with chemotherapeutic agents (e.g., capecitabine), in patients with HER2-positive breast cancer with brain metastases (5–12). However, reported clinical efficacy data were inconsistent, partly attributable to confounding factors such as the heterogeneity of patient population (e.g., stable versus progressive or previously untreated versus treated brain metastases), different treatment regimens (e.g., varying combinations and treatment cycles), or misinterpretation of intracranial and extracranial activity data. Due to the lack of prospective, randomized clinical trials to compare, side-by-side, the intracranial activity and overall efficacy of the three HER2 tyrosine kinase inhibitors, there is no consensus on the optimal HER2 inhibitor(s) for effective treatment of brain metastases in patients with HER2-positive breast cancer.

Sufficient drug penetration into the brain and brain tumors to exert pharmacologic activity is the prerequisite for intracranial activity and overall efficacy in patients with brain cancer. A better understanding of the pharmacokinetics of HER2 inhibitors in the human central nervous system (CNS) is critical to the optimal use of these drugs. Preclinical-to-clinical translation of CNS pharmacokinetics is often poor due to the biological system difference (13). Instead, *in vitro–in vivo* extrapolation-physiologically based pharmacokinetic (IVIVE-PBPK) modeling offers an innovative approach for mechanistic

[1]Karmanos Cancer Institute, Wayne State University School of Medicine, Detroit, Michigan. [2]Translational Sciences, Seagen Inc., Bothell, Washington. [3]Research, Seagen Inc., Bothell, Washington.

Corresponding Authors: Jing Li, Karmanos Cancer Institute, 4100 John R Street, HWCRC, Room 523, Detroit, MI 48201. Phone: 313-576-8258; E-mail: LiJing@wayne.edu; and Anthony J. Lee, Translational Sciences, Seagen Inc., Bothell, WA, 98021, USA. Phone: 425-527-4680; E-mail: alee@seagen.com

Clin Cancer Res 2022;28:3329–41

doi: 10.1158/1078-0432.CCR-22-0405

Translational Relevance

Small-molecule HER2 tyrosine kinase inhibitors (lapatinib, neratinib, and tucatinib) have been approved for the treatment of HER2-positive breast cancer, but there is no consensus on their efficacy in treating brain metastases. Sufficient drug brain and tumor penetration and target engagement is the prerequisite for intracranial activity and overall efficacy. A better understanding of the pharmacokinetics of HER2 inhibitors in the human central nervous system (CNS) is critical to the optimal use of these drugs. Using the *in vitro-in vivo* extrapolation, physiologically based pharmacokinetic (IVIVE-PBPK) modeling approach, supported by available clinical data, we compared, in a mechanistic and quantitative manner, the CNS pharmacokinetics and target engagement of the three HER2 inhibitors in patients with cancer. Our study sheds important pharmacologic insights into the clinical outcomes of these drugs and moreover provides critical information to guide the selection of efficacious drugs for the treatment of HER2-positive breast cancer patients with brain metastases.

prediction of drug penetration and distribution in the human brain and different tumor regions, which is otherwise difficult to be quantitatively measured in real patients due to the challenge of sampling and limitation of currently available imaging or analytic technologies. The key feature of this approach is that it allows simultaneous incorporation of system- and drug-specific parameters into a pharmacokinetic model and enables *a priori* prediction of individual *in vivo* kinetic processes by mechanistic scaling of *in vitro* data (e.g., *in vitro* enzyme and transporter kinetics) with systems data (e.g., enzyme or transporter protein abundances; refs. 14, 15).

In this study, using the IVIVE-PBPK modeling approach, supported by the existing clinical pharmacokinetic and efficacy data, we compared, in a mechanistic and quantitative manner, the CNS pharmacokinetics and target engagement of three small-molecule HER2 inhibitors (lapatinib, neratinib, and tucatinib) in patients with cancer. Our study shed important pharmacologic insights into the clinical outcomes of these drugs and moreover, provided critical information to guide selection of efficacious drug for the treatment of HER2-positive breast cancer patients with brain metastases.

Materials and Methods

In vitro studies to determine drug-specific parameters

In vitro metabolism

In vitro metabolism was determined by incubating each drug (0.5 to 50 μmol/L) with pooled human liver or intestine microsomes (0.4 mg/mL) at 37°C for 30 minutes (16). The kinetic profile of overall drug disappearance velocity versus initial drug concentrations was fitted to the Michaelis–Menton equation using nonlinear regression analysis. The *in vitro* intrinsic clearance (CL_{int}) was calculated as V_{max}/K_m, where V_{max} is maximum metabolic velocity and K_m is the substrate concentration at which 50% of V_{max} is obtained.

Binding to plasma proteins and brain tissue

Drug binding to human plasma proteins and brain tissue were determined using pooled human plasma and brain tissue samples, as described previously (17).

Passive transcellular permeability and interactions with efflux transporters

The passive transcellular permeability and interaction with efflux transporters for the three HER2 inhibitors were determined using the parental MDCKII cells and MDCKII with stable expression of ABCB1 and ABCG2, as described previously (18). Briefly, cells (3×10^4 cells per well) were seeded into 96-well transwell inserts (0.4-μmol/L pore size, polycarbonate membrane; Corning), and cultured in DMEM GlutaMAX (Gibco 10566) supplemented with 10% FBS for 5 days, with daily change of fresh medium. Bidirectional permeability experiments were performed on day 5. To determine the apical-to-basolateral (A→B) permeability, 100 μL HBSS containing the drug (1 μmol/L) was added into the top chamber and 220 μL drug-free HBSS was added into the bottom chamber. To determine the basolateral-to-apical (B→A) permeability, 100 μL drug-free HBSS was added into the top chamber and 220 μL HBSS containing the drug (1 μmol/L) was added into the bottom chamber. In addition, lucifer yellow (0.1 mg/mL; a paracellular integrity marker) was added into each top chamber. After 1-hour incubation at 37°C, samples were collected from both donor and receiver chambers. Lucifer yellow fluorescence in the receiver (bottom) chamber was measured, a permeability of < 0.03 indicating the integrity of the cell monolayer. Drug concentrations in both chambers were determined by validated LC/MS-MS methods. Bidirectional permeability experiments on the parental MDCKII and MDCKII with stable expression of ABCB1 or ABCG2 cell monolayers were carried out in the absence and presence of elacridar (0.5 μmol/L; a typical inhibitor for ABCB1) or Ko143 (1 μmol/L; a typical inhibitor for ABCG2) in the top chamber. In parallel, the positive control experiments were performed using midazolam (1 μmol/L, a marker for passive permeability), loperamide (5 μmol/L, a typical ABCB1 substrate), and gefitinib (1 μmol/L, a typical ABCG2 substrate). pH-dependent permeability experiments on the parental MDCKII, MDCKII-ABCB1, and MDCKII-ABCG2 cell monolayers were performed with the pH in the basolateral chamber adjusted to 7.4, 7.0, 6.5, or 6.0, while the pH in the apical chamber was fixed at 7.4.

Apparent permeability (P_{app} [cm/s]) was calculated as: $P_{app} = [V_r/(S \times C_0)] \times dC_r/dt$, where V_r is the volume of medium (mL) in the receiver chamber, S is the surface area (cm^2) of the cell monolayer, C_0 is the initial drug concentration (μmol/L) in the donor chamber, and dC_r/dt is the rate of drug permeation across the cell monolayer (μmol/L/s). Efflux ratio (ER) was calculated as the ratio of basolateral-to-apical apparent permeability ($P_{app,B\text{-}A}$) to apical-to-basolateral apparent permeability ($P_{app,A\text{-}B}$). Net efflux ratio was the efflux ratio in the absence of an ABCB1/ABCG2 inhibitor divided by the efflux ratio in the presence of the efflux transporter inhibitor.

PBPK model development and simulation

Model development

A whole-body PBPK model integrated with a 4-compartment permeability-limited brain (4Brain) model was developed for predicting the system and CNS pharmacokinetics of total and unbound drug, using the Simcyp Simulator V18 (Simcyp Ltd, Sheffield, United Kingdom). System-specific parameters were derived from the existing Simcyp virtual cancer patient population, unless stated otherwise.

In the whole-body PBPK model, oral absorption was predicted using the first-order absorption model with the input of the absorption rate constant estimated from observed data. Drug distribution to all organs except for the brain was perfusion rate-limited, with the steady-state volume of distribution (V_{ss}) estimated by Method 3 as implemented in the Simcyp Simulator. The whole-organ hepatic or intestinal metabolic clearance was predicted by IVIVE scaling of the *in vitro*

metabolic intrinsic clearance determined from pooled human liver or intestine microsomes (19).

The 4Brain model as implemented in the Simcyp Simulator V18 was modified to predict the CNS pharmacokinetics. The model structure and assumptions are illustrated in Supplementary Fig. S1. In brief, the 4Brain model has 4 compartments representing the brain blood, brain mass, cranial cerebrospinal fluid (CSF), and spinal CSF. Drug transport across the BBB from the brain blood to brain was governed by bidirectional passive clearance (parameterized as the passive permeability-BBB surface area product, PSB) and ABCB1- and/or ABCG2-mediated active efflux clearance. Drug transport across the blood–CSF barrier from the brain blood to cranial CSF was governed by bidirectional passive clearance (parameterized as the permeability-blood–CSF barrier surface area product, PSC) and ABCB1-mediated active influx clearance. Passive permeability allows only unbound and unionized drug to pass through all barriers, while transporters act upon unbound drug (including both unionized and ionized species). The equations describing the fluid balance and drug disposition in the 4Brain model were reported previously (20).

The PSB was estimated by scaling of the intrinsic passive permeability of unbound and unionized drug to the human brain microvasculature surface area (SA; 15 – 25 m^2) using Eq. A, where the intrinsic passive permeability is the apical-to-basolateral apparent permeability ($P_{app,A\text{-}B}$) determined from MDCKII cell monolayers at pH 7.4 normalized by unionization fraction (λ).

$$PSB = \frac{P_{app,A-B} \times SA}{\lambda} \quad (A)$$

The PSC was assumed to be half of the PSB, given the smaller surface area of the blood–CSF barrier (18, 21). The passive permeability-surface area product at the brain-CSF barrier (PSE) was fixed at 300 L/hour, assuming a high permeability of this barrier (18, 21).

In vitro ABCB1- or ABCG2-mediated intrinsic efflux clearance ($CL_{efflux,vitro}$; μL/min/mg) was estimated based on the intrinsic passive permeability (i.e., $P_{app,A\text{-}B}/\lambda$) and net efflux ratio (NER) determined from MDCKII-ABCB1 or MDCKII–ABCG2 cell monolayers, using Eq. 2 (22).

$$CL_{efflux,vitro} = \frac{2 \times P_{app,A-B} \times (NER - 1) \times SA}{\lambda \times Pro_{cell}} \quad (B)$$

where SA is the filter surface area (0.143 cm^2) of a 96-well transwell, and Pro_{cell} is the cell membrane protein amount (mg) of MDCKII-ABCB1or MDCKII–ABCG2 cells in a 96-well transwell.

In vivo ABCB1- or ABCG2-mediated efflux clearance at the BBB ($CL_{efflux,BBB,}$) was scaled from the $CL_{efflux,vitro}$ using Eq. (C).

$$CL_{efflux,BBB} = CL_{efflux,vitro} \times RAF = CL_{efflux,vitro} \times \frac{\text{Abundance } in\ vivo}{\text{Abundance } in\ vitro} \times BMvPGB \times BW \quad (C)$$

where RAF represents the transporter *in vivo-in vitro* relative activity factor; abundance *in vivo* and *in vitro* represents the transporter protein abundance in human brain microvessels (pmol/mg microvessles) and in MDCKII-ABCB1 or –ABCG2 cell membranes (pmol/mg cell membrane), respectively; BMvPGB is the milligrams of microvessels per gram of brain; and BW is the human brain weight.

ABCB1 has been located at the apical (CSF facing) membrane of the blood–cranial CSF barrier, and therefore ABCB1-mediated active influx from the blood to cranial CSF was considered at the blood–cranial CSF barrier. However, ABCB1 protein abundance data at this barrier is not available, and thus the RAF for ABCB1-mediated active influx clearance at the blood–CSF barrier was assigned, which was validated in our previous study using observed clinical ribociclib CSF data (23) as well as in the present study with observed clinical tucatinib CSF data.

Model simulation

The total and unbound drug concentration – time profiles of each HER2 inhibitor in the plasma, brain, and CSF were simulated in the Simcyp virtual cancer population (10 trials with 10 subjects in each trial). The dosing regimens for simulations were matched to the United States Food and Drug Administration (FDA)-approved standard dosing regimens. Specifically, tucatinib was given orally at 300 mg twice daily on a 3-weeks-on continuous schedule; lapatinib was given orally at 1,250 mg once daily on a 3-weeks-on continuous schedule; neratinib was given orally at 240 mg once daily on a 3-weeks-on continuous schedule. The developed PBPK models were verified by comparing the model-simulated plasma and CNS pharmacokinetics with the observed clinical plasma and CNS pharmacokinetic data (if available).

To understand the heterogeneity of drug penetration into the brain and brain tumors, simulations of unbound drug concentration – time profiles of each HER2 inhibitor were performed for the normal brain (i.e., with brain pH 7.12, intact tight junctions, and ABCB1 protein abundance 3.38 pmol/mg and ABCG2 6.21 pmol/mg at the BBB) and hypothesized brain metastasis tumors (with a relatively acidic tumor pH and varying degrees of disrupted BBB) in the Simcyp virtual cancer population (10 trials with 10 subjects in each trial). Specifically, the hypothesized metastasis tumors included tumor A (with brain pH 6.5, and intact BBB), tumor B (with brain pH 6.5, intact tight junctions, and complete loss of ABCB1 and ABCG2 expression at the BBB), and tumor C (with brain pH 6.5, leaky tight junctions leading to 5-fold increase of passive permeability, and complete loss of ABCB1 and ABCG2 expression at the BBB).

Data Availability Statement

The data generated in this study are available within the article and its Supplementary Data files.

Results

Passive transcellular permeability and interaction with ABCB1 and ABCG2

Passive transcellular permeability and *in vitro* ABCB1- and ABCG2-mediated intrinsic efflux clearance for the three HER2 inhibitors were determined using the transwell system with the parental MDCKII cell monolayer and MDCKII cells with stable expression of human ABCB1 and ABCG2 (18). The apical-to-basolateral apparent transcellular passive permeability ($P_{app,A\text{-}B}$; at pH 7.4), intrinsic passive transcellular permeability ($P_{app,A\text{-}B}/\lambda$), efflux ratio, and net efflux ratio are summarized in Supplementary Table S1. Notably, while the three HER2 inhibitors are weak base drugs, they exhibit different acid dissociation (or ionization) constant (PK_a; **Table 1**). Based on pH partition theory (Henderson-Hasselbalch equation), the estimated unionization fraction (λ) at pH 7.4 was 0.947, 0.613, and 0.360 for tucatinib, lapatinib, and neratinib, respectively. Given the notion that only unbound and unionized drug pass through biological membranes, the intrinsic passive transcellular permeability ($P_{app,A\text{-}B}/\lambda$) for unbound and unionized drug was estimated as 13.3×10^{-6},

Table 1. Drug-specific parameters used in the development of whole-body-4Brain PBPK models.

	Tucatinib	Lapatinib	Neratinib	Comments/Reference
Physicochemical				
MW (g/mol)	480	581	557	PubChem
LogP	3.82	5.10	4.90	ChemAxon
Weak base (PKa1, PKa2)	4.18, 6.15	3.80, 7.20	4.66, 7.65	ChemAxon
B/P	0.93	0.7	0.7	Experimental determined
$f_{u,p}$	0.030	0.014	0.007	Experimental determined
Absorption				
fa	0.5	0.5	0.2	Assigned based on observed data
Ka	0.8	0.3	0.25	Observed
Lag time (h)	0.6	0.5	0.8	Observed
fu_{gut}	0.0035	0.00038	0.0013	Simcyp predicted
Q_{gut} (L/hour)	13.8	5.21	8.32	Simcyp predicted
Distribution				
V_{ss} (L/kg)	6.58	50.3	10.9	Predicted by Method 3, K_p scalar of 1
Elimination				
Human liver microsomes				
CL_{int} (μL/min/mg)	41.8	22.8	39.0	Experimental determined from HLM
fu_{inc}	0.17	0.17	0.17	Assigned
Human intestinal microsomes				
CL_{int} (μL/min/mg)	4.50	5.66	24.6	Experimental determined from HIM
fu_{mic}	0.2	0.2	0.2	Assigned
CL_R (L/hour)	6	2	2	Assigned based on observed urine data
Other system clearance (L/hour)	0	0	30	Assigned based on observed data
4Brain model				
BBB				
PSB (L/hour)	9.55	2.98	9.74	Estimated by Eq. (A)[a]
$f_{u,br}$	0.015	0.0004	0.004	Experimental determined from human brain tissue
$CL_{ABCB1,vitro}$ (μL/min/mg)	1245	216.9	354.2	Experimental determined Eq. (B)[b]
$CL_{ABCG2,vitro}$ (μL/min/mg)	657	44.5	113.4	Experimental determined Eq. (B)[b]
ABCB1 RAF at BBB	87.3	87.3	87.3	Determined based on ABCB1 abundance in normal human brain microvessels in Eq.(C)[c]
ABCG2 RAF at BBB	125.3	125.3	125.3	Determined based on ABCG2 abundance in normal human brain microvessels in Eq.(C)[c]
Blood–CSF barrier				
PSC (L/hour)	4.78	1.5	4.87	Assumed to be half of PSB
fu_{csf}	1	1	1	Assigned given low CSF protein concentration
$CL_{ABCB1,vitro}$ (μL/min/mg)	1,245	216.9	354.2	Experimental determined Eq. (B)[b]
ABCB1 RAF at BCCSF	8.73	8.73	8.73	Assigned and validated by observed CSF data
Brain–cranial CSF barrier				
PSE (L/hour)	300	300	300	Assigned assuming no barrier function

Abbreviations: B/P, blood-to-plasma partition ratio; $CL_{ABCB1,vitro}$ and $CL_{ABCB1,vitro}$, ABCB1- and ABCG2-mediated *in vitro* efflux clearance, respectively; CL_{int}, *in vitro* intrinsic metabolic clearance; CL_R, renal clearance; $f_{u,br}$, fraction unbound drug in brain tissue; $f_{u,p}$, fraction of unbound drug in plasma; fu_{csf}, fraction unbound in CSF; fu_{gut}, fraction of unbound drug in enterocytes; fu_{mic}, fraction of unbound in microsomal incubation; K_m, substrate concentration at which half of V_{max} is achieved; logP, logarithm of the neutral species octanol-to-buffer partition ratio; MW, molecule weight; PK_a, acid dissociation constant; PSB, passive permeability-surface area product at the BBB; PSC, passive permeability-surface area product at the blood–cranial CSF barrier; PSE, passive permeability-surface area product at the brain-cranial CSF barrier; Q_{gut}, gut blood flow; RAF, *in vivo-in vitro* relative activity factor; V_{max}, maximum metabolic rate; V_{ss}, volume of distribution at steady-state.

[a] $PSB = \frac{P_{app,A-B} \times SA}{\lambda}$ (Eq. A), where $P_{app,A\rightarrow B}$ is the apparent permeability determined from MDCKII cell monolayer; SA is the human brain microvasculature surface area (mean, 20 m^2); and λ is unionization efficiency.

[b] $CL_{efflux,vitro} = \frac{2 \times P_{app,A-B} \times (NER -- 1) \times SA}{\lambda \times Pro_{cell}}$ (Eq. B), where $CL_{efflux,vitro}$ (μL/min/mg) is the *in vitro* efflux transporter-mediated intrinsic clearance; NER is the net efflux ratio determined from MDCKII-ABCB1or MDCKII–ABCG2; $P_{app,A-B}$ is the apparent passive permeability determined from MDCKII; SA is the filter surface area (0.143 cm^2) in a 96-well transwell; λ is unionization efficiency; and Pro_{cell} is the cell membrane protein amount in a 96-well transwell.

[c] $CL_{efflux,BBB} = CL_{efflux,vitro} \times RAF = CL_{efflux,vitro} \times \frac{Abundance\ in\ vivo}{Abundance\ in\ vitro} \times BMvPGB \times BW$ (Eq. C) where RAF is the relative activity factor; BMvPGB is the milligrams of brain microvessels per gram brain; BW is the average human brain weight; abundance *in vivo* or *in vitro* represents the ABCB1/ABCG2 transporter protein expression level in human brain microvessels or in MDCKII-ABCB1 and –ABCG2 cells, respectively.

4.14×10^{-6}, and 13.5×10^{-6} cm/s for tucatinib, lapatinib, and neratinib, respectively (Supplementary Table S1). These values were then scaled to human brain microvasculature surface area (Eq. 1 in **Table 1**) to predict the BBB passive permeability clearance (PSB) of the unbound and unionized drug in the PBPK models (**Table 1**).

The three HER2 inhibitors were the substrates for ABCB1 and ABCG2. Tucatinib showed the highest ABCB1- and ABCG2-mediated efflux efficiency (net efflux ratio, 13.74 and 7.71), followed by lapatinib (8.12 and 2.46) and neratinib (4.56 and 2.14; Supplementary Table S1). Based on the $P_{app,A\text{-}B}$/ λ and net efflux ratio

(Eq. 2 in **Table 1**), *in vitro* ABCB1 intrinsic efflux clearance was determined as 1,245, 217, and 354 μL/min/mg for tucatinib, lapatinib, and neratinib, respectively; and the respective *in vitro* ABCG2 intrinsic efflux clearance was 657, 44, and 113 μL/min/mg (**Table 1**). These values were then scaled to BBB transporter protein abundance, brain microvessel density, and brain weight (Eq. 3 in **Table 1**) to predict that ABCB1- and ABCG2-mediated *in vivo* efflux clearance at the human BBB (23). Overall, the transporter-mediated efflux clearance at the normal BBB in the average population was estimated as 11.46 L/hour for tucatinib, 1.47 L/hour for lapatinib, and 2.71 L/hour for neratinib.

Notably, similar to other weak base drugs (e.g., AZD1775, ribociclib, palbociclib, and abemaciclib; 18, 23), the three HER2 inhibitors exhibited pH-dependent apparent permeability and efflux ratio across the MDCKII, MDCKII-ABCB1, and MDCKII-ABCG2 cell monolayers (Supplementary Fig. S2). As the pH was decreasing (7.4, 7.0, 6.5, and 6.0) in the basolateral chamber (mimicking brain/brain tumor interstitium) while remaining the same pH (7.4) in the apical chamber (mimicking blood circulation), the apparent permeability increased in the apical-to-basolateral direction while decreasing in the basolateral-to-apical direction, collectively resulting in a lower efflux ratio at a relatively acidic basolateral pH (Supplementary Fig. S2). This observation was supported by the pH partition theory suggesting that at a relatively acidic basolateral pH, the ionization of a weak base drug was increased, thereby leading to a decrease in the basolateral-to-apical permeability and trap of ionized drugs in the basolateral compartment. These *in vitro* data could be translated to *in vivo*, implying that the relatively acidic tumor environment would facilitate tumor penetration of weak base drugs including the three HER2 inhibitors.

PBPK modeling and simulation

Tucatinib PBPK model verification

The whole-body-4Brain PBPK model for prediction of tucatinib plasma and CNS pharmacokinetics was verified by comparing model-simulated plasma and CSF data with observed clinical data from two clinical studies (ONT-380–004 and TBCRC049), in which patients with metastatic HER2-positive breast cancer were treated with tucatinib (300 mg twice daily), trastuzumab, and capecitabine (24, 25). The model well predicted tucatinib mean plasma concentration time profiles and inter-individual variabilities, as demonstrated by > 98% of observed plasma concentration data falling within the 5th and 95th percentiles of the simulated population mean plasma time profile (**Fig. 1**).

Tucatinib cranial CSF concentrations were reported from 13 patients with HER2-positive metastatic breast cancer who were treated with tucatinib (300 mg twice daily), trastuzumab, and capecitabine (TBCRC049 study; ref. 24). The PBPK model reasonably well predicted the observed tucatinib CSF data, as demonstrated by > 95% observed data falling within the 5th and 95th percentiles of the simulated population mean profile (**Fig. 1**). Specifically, following the 1st dose (cycle 1 day 1) and 42nd dose (cycle 2, day 1), the model-predicted population mean cranial CSF C_{max} of tucatinib was 12.2 nmol/L and 20.1 nmol/L, respectively, and the respective T_{max} was 4.3 and 2.9 h. These data were consistent with the observed CSF concentrations at 2–5 hours postdosing on cycle 1 day 1 (mean, 10.9 nmol/L) and cycle 2 day 1 (mean, 21.6 nmol/L) in 13 patients (24). In addition, the model-predicted population mean CSF-to-unbound plasma ratio (CSF $K_{p,uu}$) was 0.65 and 0.75 following the 1st dose and 42th dose, respectively, in agreement with the observed CSF $K_{p,uu}$ on cycle

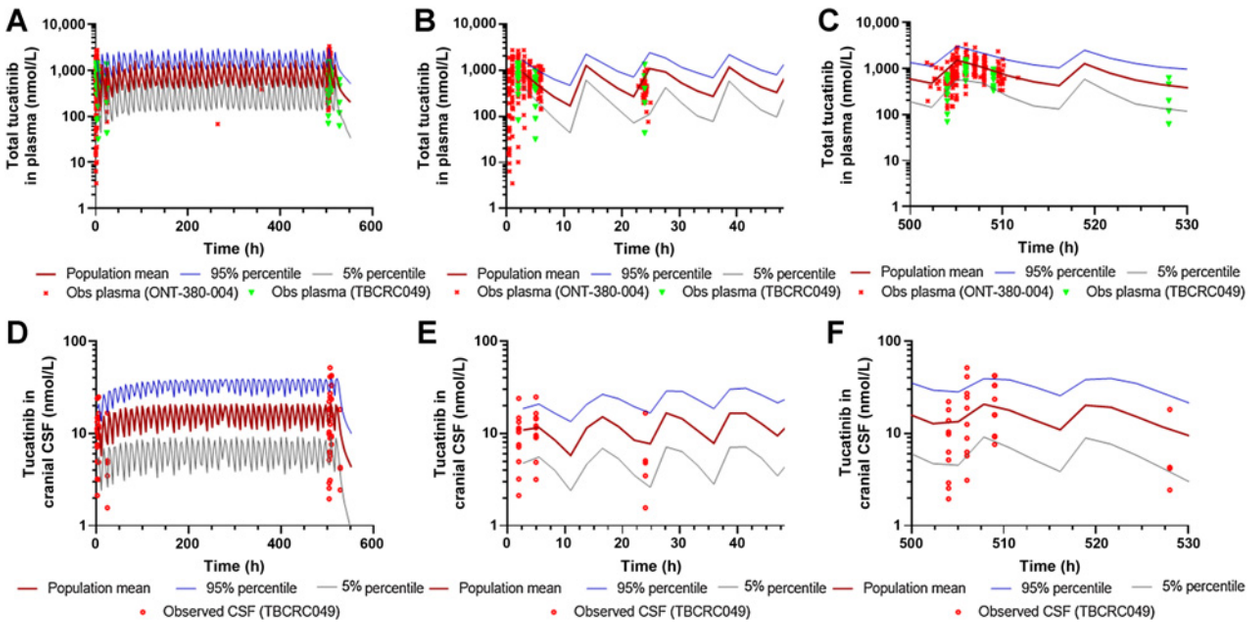

Figure 1.

PBPK model-simulated and clinically observed tucatinib concentration time profiles in the plasma (**A–C**) and CSF (**D–F**) in patients with cancer. Simulations of 10 trials with 10 subjects in each were performed in the Simcyp virtual cancer patient population following 22-day (528 hours) tucatinib treatment (300 mg twice daily). Observed clinical plasma pharmacokinetic data were obtained from two clinical studies (ONT-380–004 and TBCRC049), in which patients with metastatic HER2-positive breast cancer were treated with tucatinib [300 mg twice daily (BID)], and observed CSF data were obtained from TBCRC049 study. The solid red line represents population mean plasma or CSF concentration–time profile; gray and blue lines represent the 5th and 95th percentiles of the mean concentration profile, respectively; orange and green symbols represent observed concentration data in patients. BID, twice daily

1 day 1 (geometric mean, 0.51; range, 0.16–1.86) and cycle 2 day 1 (geometric mean, 0.76; range, 0.18–2.02) in 13 patients (24).

Lapatinib PBPK model verification

The model-simulated plasma, brain, and CSF concentration – time profiles of total or unbound lapatinib following a single dose or 1 cycle of treatment (1,250 mg once daily, 21 days) are illustrated in **Fig. 2** and Supplementary Fig. S3. The developed PBPK model adequately predicted lapatinib plasma pharmacokinetics, as verified by the comparison of the model-predicted mean population plasma pharmacokinetic parameters with the observed parameters reported on the FDA-approved drug label. Specifically, following chronic treatment with oral lapatinib (1,250 mg, once daily) in patients with cancer, the predicted versus observed population mean apparent oral clearance (CL/F) was 31.7 versus 34.5 L/hour (predicted/observed ratio, 0.92), effective elimination half-life ($T_{1/2}$) was 22.1 versus 24.0 hours (ratio, 0.92), and apparent volume of distribution (V/F) was 1,011 versus 1,194 L (ratio, 0.85).

Interestingly, lapatinib plasma concentration reached the steady-state following 1 cycle of treatment (1,250 mg once daily, 21 days); whereas, the brain and CSF concentrations continued increasing without reaching the steady-state until 5 cycles of treatment (1,250 mg once daily, 105 days), and as the result, the brain or CSF $K_{p,uu}$ continued increasing and eventually approached 1.0 at the steady-state

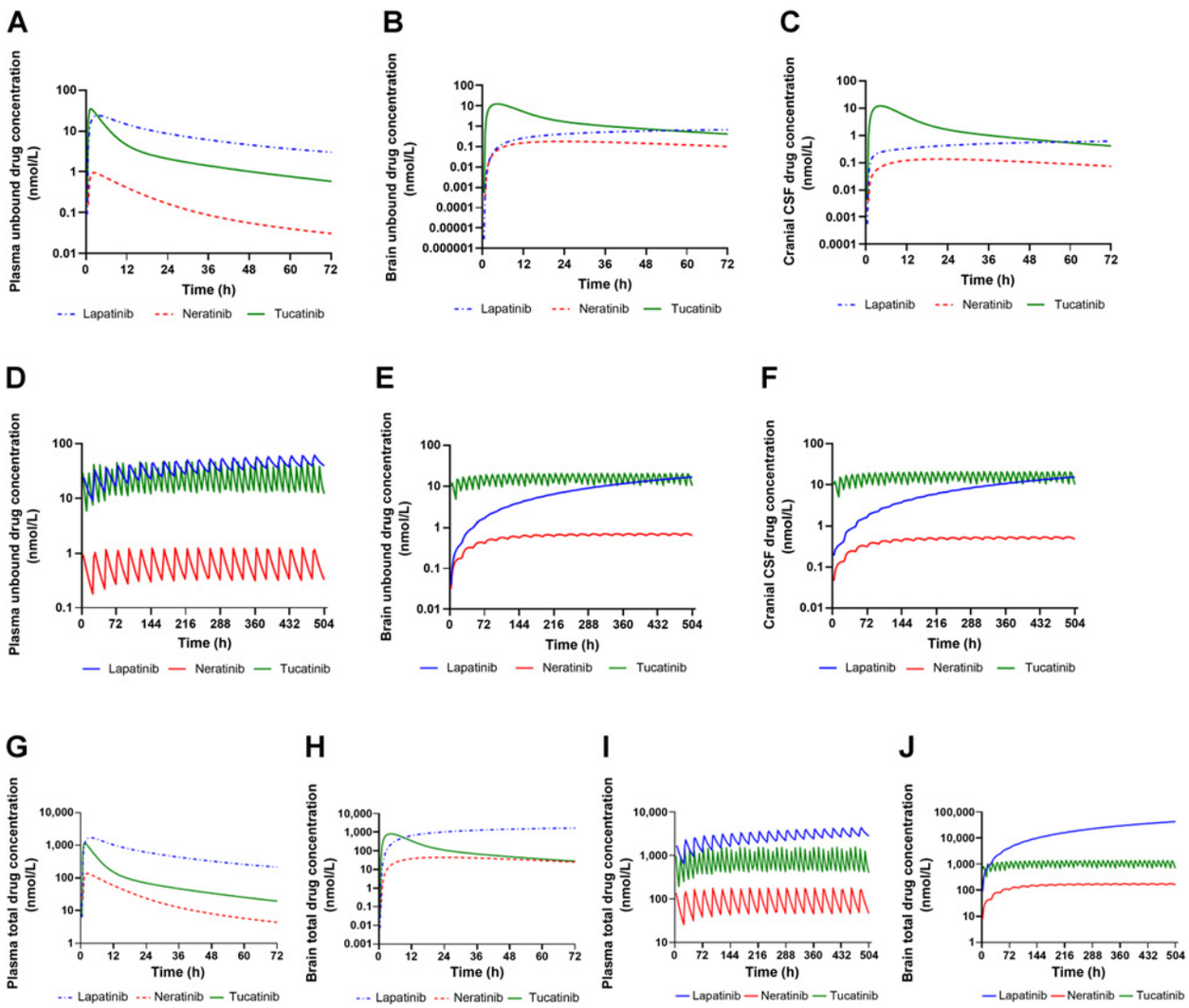

Figure 2.

Model-simulated population mean plasma, brain, and CSF concentration – time profiles of the three HER2 inhibitors following a single dose or 1 cycle (21 days) of treatment. **A–C,** Simulated mean unbound drug – concentration time profiles in the plasma, brain, and CSF follow a single oral dose (lapatinib, 1,250 mg; neratinib, 240 mg; tucatinib, 300 mg). **D–F,** Simulated mean unbound drug – concentration time profiles in the plasma, brain, and CSF follow 1 cycle (21 days/504 hours) of treatment (lapatinib, 1,250 mg once daily; neratinib, 240 mg once daily; tucatinib, 300 mg twice daily). **G** and **H,** Simulated mean total drug–concentration time profiles in the plasma and brain following a single oral dose (lapatinib, 1,250; mg, neratinib, 240 mg; tucatinib, 300 mg). **I** and **J,** Simulated mean total drug–concentration time profiles in the plasma and brain following 1 cycle (21 days/504 hours) of treatment (lapatinib, 1,250 mg once daily; neratinib, 240 mg once daily; tucatinib, 300 mg twice daily). Simulations of 10 trials with 10 subjects in each were performed in the Simcyp virtual cancer patient population. BID, twice daily; QD, once daily.

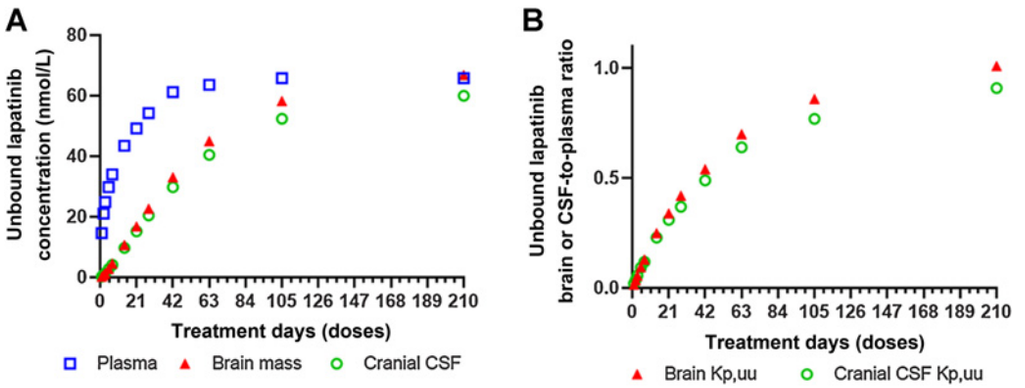

Figure 3.

Accumulation of lapatinib in the human CNS following chronic treatment. **A,** Increase of unbound lapatinib concentrations in the plasma, brain, and CSF with the increase of treatment days (doses). **B,** Increase of unbound lapatinib brain- or CSF-to-plasma ratio ($K_{p,uu}$) with the increase of treatment days (doses).

(**Fig. 3**). Limited clinical CNS pharmacokinetic data of lapatinib were available in patients. Notably, the model-predicted lapatinib accumulation in the CNS following chronic treatment was recapitulated by the observed data in 4 patients receiving 2, 3, or 5 doses (1,250 mg once daily), whereby lapatinib concentrations in resected brain metastases were increased by 64-fold as doses increased from 2 to 5 (26). In another study, lapatinib CSF concentrations were determined as 2.2 and 7.7 nmol/L at 5 hours after an oral dose (1,250 mg) in two patients with HER2-positive breast cancer brain metastasis (27), and accordingly the estimated CSF $K_{p,uu}$ was 0.061 and 0.092 assuming lapatinib fraction unbound in plasma was 0.014. Given the CNS accumulation of lapatinib with the treatment days (or doses), a direct comparison of the observed and model-predicted lapatinib CSF data was not feasible due to the lack of information on the exact number of treatment days that the two patients received before the CSF sample collection. Regardless, the observed lapatinib CSF data were in line with the model-predicted mean CSF concentration (1.42 – 9.74 nmol/L) and CSF $K_{p,uu}$ (0.057 – 0.23) following 3 to 14 days of treatment (1,250 mg once daily; **Fig. 3**).

Neratinib PBPK model verification

The model-simulated plasma, brain, and CSF concentration – time profiles of total or unbound neratinib following a single dose or 1 cycle of treatment (240 mg once daily, 21 days) are presented in **Fig. 2**; Supplementary Fig. S3. The model adequately predicted neratinib plasma pharmacokinetics, as verified by the comparison of the model-predicted mean population plasma pharmacokinetic parameters with the observed parameters reported on the FDA-approved drug label. Specifically, following chronic treatment with oral neratinib (240 mg, once daily) in patients with cancer, the predicted versus observed population mean CL/F was 220 versus 216 L/hour (predicted/observed ratio, 1.02), $T_{1/2}$ was 15.1 versus 14.6 hours (ratio, 1.03), and V/F was 4,792 versus 6,433 L (ratio, 0.75).

Notably, the plasma and CNS exposure of unbound neratinib appeared low, with the model-predicted mean steady-state unbound neratinib concentrations of 0.66, 0.68 and 0.51 nmol/L in the plasma, brain, and cranial CSF, respectively (**Fig. 2** and **Table 2**). Sparse neratinib CNS concentration data were reported from 3 patients with HER2-positive breast cancer brain metastasis following 1 to 225 weeks of treatment (240 mg once daily). In all 3 patients, neratinib CSF concentrations were below the lower limited of quantitation (< 1 nmol/L) and total neratinib plasma concentrations measured in 2 patients were 61.6 and 96.6 nmol/L (corresponding to unbound plasma concentrations of 0.43 and 0.67 nmol/L assuming the fraction unbound in plasma was 0.007; ref. 28). Collectively, the observed neratinib plasma and CSF data were in agreement with the model prediction.

Comparison of the CNS pharmacokinetics of the three HER2 inhibitors

The three HER2 inhibitors exhibited different CNS pharmacokinetics with respect to the rate and extent of BBB penetration and the time to reach the CNS steady-state (**Fig. 2**). Analogous to the concept of drug oral absorption, the rate of BBB penetration can be assessed by the time ($T_{max,br}$) to achieve the maximum drug brain concentration ($C_{max,br}$). The rate of BBB penetration is largely driven by the extent of drug binding to brain tissue as well as the passive and active efflux clearance at the BBB. Specifically, higher brain tissue binding (i.e., lower fraction unbound in the brain) and lower passive and active efflux clearance at the BBB lead to slower BBB penetration (18). Tucatinib fraction unbound in brain tissue ($f_{u,br}$, 0.015) was 3.75- and 37.5-fold of that for neratinib (0.004) and lapatinib (0.0004), respectively. In addition, the overall BBB passive and active efflux clearance of tucatinib (PSB+ $CL_{efflux,BBB}$, 21.0 L/hour) was 1.68- and 4.72-fold of that for neratinib (12.4 L/hour) and lapatinib (4.45 L/hour), respectively. Therefore, as expected and model predicted, tucatinib showed the quickest brain penetration ($T_{max,br}$, 2.9 hours), followed by neratinib ($T_{max,br}$, 11.4 hours) and lapatinib ($T_{max,br}$, > 24.0 hours; **Table 2**). It should be noted that due to the remarkedly slow BBB penetration of lapatinib, its disposition (i.e., terminal half-life) in the brain was mainly limited by the rate of BBB penetration instead of elimination, a "flip-flop" phenomenon similar to the plasma pharmacokinetic profile of a slow-released oral drug formulation where the terminal half-life reflects the half-life of the absorption but not elimination. Thus, given the significantly prolonged brain terminal half-life (due to slow BBB penetration) and relatively shorter plasma half-life, lapatinib continued to accumulate in the brain and CSF without reaching the steady-state until 5 cycles (105 days) of treatment (**Fig. 3**).

The extent of drug BBB penetration is commonly assessed by the unbound drug brain-to-plasma partition coefficient ($K_{p,uu}$), which is estimated as the steady-state unbound drug brain-to-plasma concentration ratio or area under concentration-time curve (AUC) ratio. In

Table 2. PBPK model-predicted unbound drug plasma and CNS pharmacokinetics at the steady-state following one-cycle treatment of the three HER2 inhibitors at the standard dosing regimens[a].

	Tucatinib (300 mg BID, 21 days)	Lapatinib (1,250 mg QD, 21 days)	Neratinib (240 mg QD, 21 days)
Plasma			
$T_{ss,max}$ (h)	2.9	3.8	3.8
$C_{ss,max}$ (nmol/L)	37.6	60.8	1.16
$C_{ss,min}$ (nmol/L)	12.1	39.3	0.33
$C_{ss,ave}$ (nmol/L)	22.5	49.3	0.66
AUC_{24h} (nmol/L/hour)	606	1,321	18.0
Brain			
$T_{ss,max}$ (h)	2.9	24.0	11.4
$C_{ss,max}$ (nmol/L)	19.9	16.8	0.72
$C_{ss,min}$ (nmol/L)	10.2	16.8	0.65
$C_{ss,ave}$ (nmol/L)	14.5	16.8	0.68
AUC_{24h} (nmol/L/hour)	456	453	19.0
Brain $K_{p,uu}$[b]	0.65	0.34	1.06
TER for HER2[c]	2.1	0.15	0.12
TER for EGFR[c]	0.032	0.35	0.38
Cranial CSF			
$T_{ss,max}$ (h)	2.9	21.5	8.9
$C_{ss,max}$ (nmol/L)	20.1	15.3	0.54
$C_{ss,min}$ (nmol/L)	10.1	15.2	0.48
$C_{ss,ave}$ (nmol/L)	14.5	15.2	0.51
AUC_{24h} (nmol/L/hour)	456	416	14.3
CSF $K_{p,uu}$[d]	0.65	0.31	0.80
Spinal CSF			
$T_{ss,max}$ (hour)	5.4	24.0	11.4
$C_{ss,max}$ (nmol/L)	18.6	15.0	0.54
$C_{ss,min}$ (nmol/L)	11.8	15.0	0.49
$C_{ss,ave}$ (nmol/L)	14.9	15.0	0.51
AUC_{24h} (nmol/L/hour)	464	405	14.3
CSF $K_{p,uu}$[d]	0.66	0.31	0.79

Abbreviations: BID, twice daily; $C_{ss,max}$, maximum steady-state concentration; $C_{ss,min}$, trough steady-state concentration; $C_{ss,ave}$, average steady-state concentration; AUC_{24h}, area under the concentration–time curve during 24 hours at the steady-state; QD, once daily.

[a]Simulations of 10 trials with 10 subjects in each trial were performed in the Simcyp cancer patient population. Data are presented as the population mean values.

[b]Brain $K_{p,uu}$ is estimated as the brain-to-plasma AUC_{24h} ratio of the unbound drug at the steady-state.

[c]TER (target engagement ratio) is calculated as the ratio of the average steady-state unbound brain concentrations to the *in vitro* IC_{50} for inhibiting HER2 or EGFR enzymes.

[d]CSF $K_{p,uu}$ is estimated as the CSF-to-plasma AUC_{24h} ratio of the unbound drug at the steady-state.

general, the $K_{p,uu}$ is determined by the relative contribution of passive clearance and transporter-mediated active clearance at the BBB. If the BBB transport of a drug is dominated by passive permeability, the $K_{p,uu}$ would approach 1; whereas, when a drug is actively transported by efflux or uptake transporters at the BBB, the $K_{p,uu}$ would be smaller or larger than 1.0. PBPK model predicted that following 1 cycle of standard treatment, the brain penetration of tucatinib and neratinib reached the steady-state with the $K_{p,uu}$ of 0.75 and 1.06, respectively; whereas, the $K_{p,uu}$ of lapatinib continued increasing (e.g., from 0.34 after 1-cycle treatment to 0.70 after 3-cycle treatment) and eventually approached 1.0 at the steady-state after 5 cycles of treatment (**Fig. 3**). The IVIVE predicted that the ratio of the BBB passive clearance (PSB) to active efflux clearance ($CL_{efflux,BBB}$) was 0.83 for tucatinib, 2.03 for lapatinib, and 3.59 for neratinib, suggesting that the BBB transport of tucatinib was relatively dominated by active efflux, while the BBB transport of lapatinib and neratinib was mainly governed by passive clearance. It was therefore expected that tucatinib showed a $K_{p,uu} < 1.0$ while neratinib and lapatinib reached a $K_{p,uu}$ of ~ 1 at the steady-state.

Of note, PBPK model simulations suggested that for each HER2 inhibitor, the CSF and brain pharmacokinetic profiles were similar, and the mean CSF-to-unbound plasma ratio (CSF $K_{p,uu}$) was close to brain $K_{p,uu}$ (**Fig. 2** and **Table 2**). Drug penetration from the circulation blood to CSF is controlled by the blood–CSF barrier, which is formed by the choroid plexus epithelial cells and the arachnoid membrane (29). ABCB1 expression has been identified on the apical, CSF-facing side of the blood–CSF barrier, suggesting that ABCB1 may facilitate the transport of substrates into the CSF (30, 31). The IVIVE predicted that ABCB1-mediated *in vivo* efflux clearance at the blood–CSF barrier was 0.65, 0.11, and 0.18 L/hour for tucatinib, lapatinib, and neratinib, respectively, accounting for 14%, 8%, and 4% of their respective passive clearance at the blood–CSF barrier (PSC; **Table 1**), indicating an insignificant role of ABCB1 in the CSF penetration of the three HER2 inhibitors. Therefore, CSF concentrations could be used as the surrogates of unbound drug brain concentrations for the three HER2 inhibitors.

Unbound drug exposure in the human normal brain and brain metastases

While the $K_{p,uu}$ is a key parameter as the measure of the extent of drug brain penetration, it is the unbound drug brain/tumor concentration to drive pharmacologic activity and efficacy, which is determined by both the $K_{p,uu}$ and systemic (or plasma) drug exposure.

Notably, although the extent of brain penetration of neratinib ($K_{p,uu}$, 1.06) was larger than tucatinib ($K_{p,uu}$, 0.75) and lapatinib ($K_{p,uu}$, 0.34) following 1 cycle of standard dosing, the brain exposure to unbound neratinib ($C_{ss,ave,br}$, 0.68 nmol/L) was about 20-fold lower as compared to the other two HER2 inhibitors ($C_{ss,ave,br}$, 14.5 for tucatinib and 16.8 nmol/L for lapatinib; **Fig. 2**; **Table 2**). The significantly lower unbound neratinib brain exposure was indeed driven by its low unbound drug plasma exposure. For example, the population mean plasma $C_{ss,ave}$ of unbound neratinib (0.66 nmol/L) was only 2.9% and 1.3% of that for unbound tucatinib (22.5 nmol/L) and lapatinib (49.3 nmol/L), respectively, following 1 cycle of standard doing (**Table 2**). Hence, in spite of excellent BBB penetration (with $K_{p,uu} \sim 1$), neratinib was unlikely to achieve adequate pharmacologic concentration for target inhibition in the brain following the standard dosing regimen. These data underscore the importance for consideration of not only the extent of brain penetration ($K_{p,uu}$) but also drug plasma exposure (that could be achieved at a safe or tolerable dose) when selecting a candidate drug for brain cancer treatment.

The disruption of physical and biochemical barriers of the BBB in brain metastases could lead to increased drug tumor penetration, especially for ABCB1 and ABCG2 substrate drugs. As revealed by quantitative proteomics, the human normal BBB expresses ABCB1 and ABCG2 at a median protein abundance of 3.38 and 6.21 pmol/mg, respectively; whereas, the protein expression of these two major efflux transporters is remarkedly reduced or lost in isolated microvessels of the majority ($\sim$ 90%) of human breast cancer brain metastasis specimens (20, 32). In addition, it is known that the extracellular pH in human brain tumors is relative acidic (as low as 5.9 with a mean around 6.8) as compared to the human normal brain ($\sim$ 7.1 – 7.2; refs. 33–35). The regional pH difference in the normal brain and brain tumors could

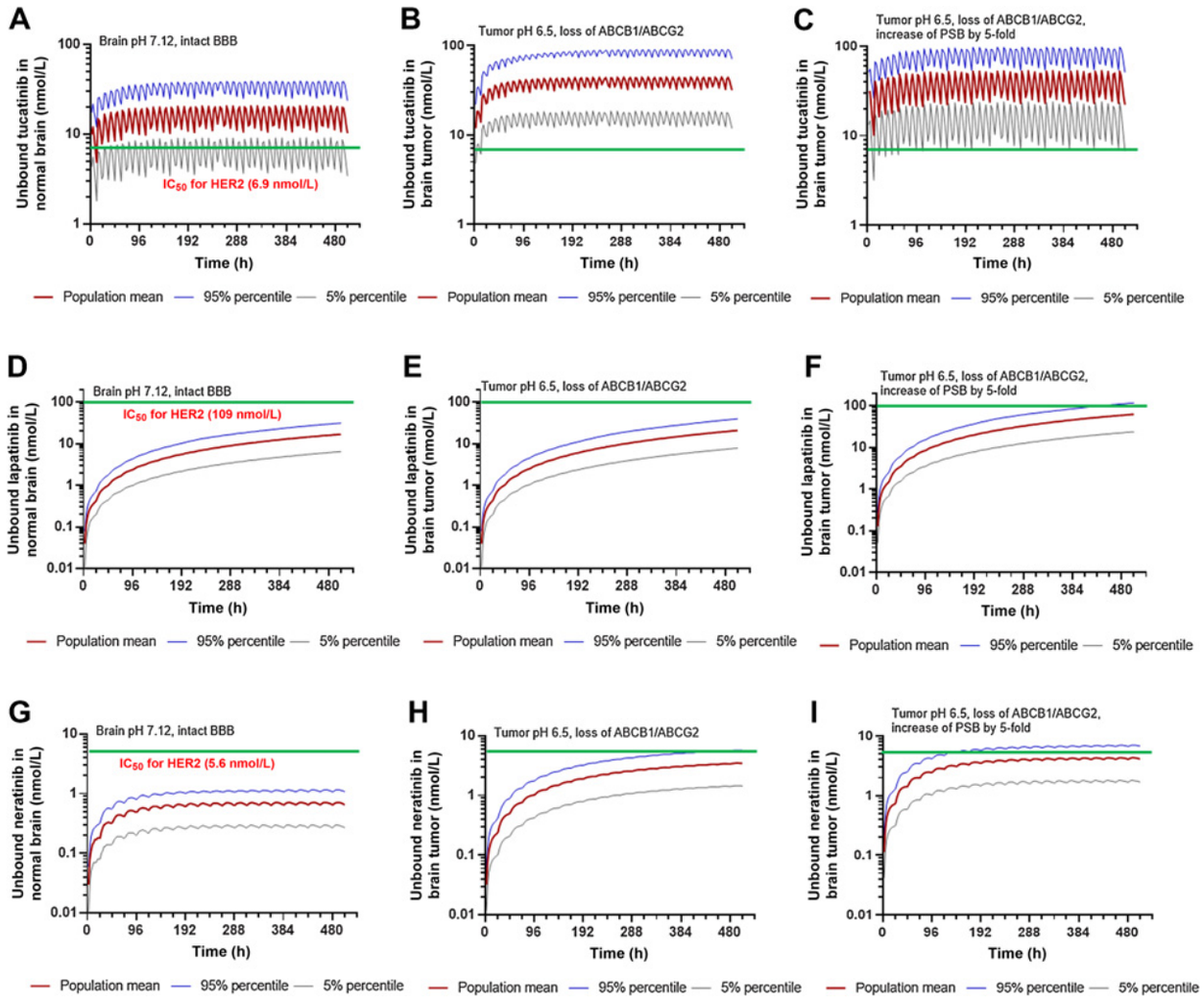

Figure 4.

Model-simulated unbound drug–concentration time profiles of tucatinib (**A**–**C**), lapatinib (**D**–**F**), and neratinib (**G**–**I**) in the normal brain (with brain pH 7.2 and intact BBB) and hypothesized brain metastasis tumors (with relatively acidic pH and disrupted BBB) following 1 cycle (21 days/504 hours) of treatment (tucatinib, 300 mg twice daily; lapatinib, 1,250 mg once daily; neratinib, 240 mg once daily). Simulations were performed in the Simcyp virtual cancer patient population (10 trials with 10 subjects in each trial). The solid red lines represent population mean plasma concentration-time profiles; gray and blue lines represent the 5th and 95th percentiles of the mean concentration profile, respectively. Green lines represent the *in vitro* IC_{50} for HER2 inhibition. BID, twice daily; QD, once daily.

contribute to the heterogeneous brain and tumor distribution of weak base drugs, as demonstrated by the *in vitro* pH-dependent apparent permeability and efflux ratio (Supplementary Fig. S2).

Model simulations demonstrated heterogeneous drug exposure in the hypothesized metastasis tumors, including tumor A (i.e., with brain pH 6.5, and intact BBB), tumor B (i.e., with brain pH 6.5, intact tight junctions, and loss of ABCB1 and ABCG2 expression at the BBB), and tumor C (i.e., with brain pH 6.5, leaky tight junctions leading to 5-fold increase of passive permeability, and loss of ABCB1 and ABCG2 expression at the BBB; **Fig. 4**). Following one-cycle treatment of tucatinib (300 mg twice daily, 21 days), the simulated population mean $C_{ss,ave}$ of unbound tucatinib in tumor A (16.6 nmol/L), tumor B (35.1 nmol/L), and tumor C (37.5 nmol/L) was 1.1-, 2.4-, and 2.6- fold of that in the normal brain (14.5 nmol/L), respectively; and the respective $K_{p,uu}$ was 0.74, 1.75, and 1.91 in tumors A, B, and C as compared to 0.65 in the normal brain (**Fig. 4**). Following one-cycle treatment of lapatinib (1,250 mg once daily, 21 days), the simulated population mean $C_{ss,ave}$ of unbound lapatinib in tumor A (20.8 nmol/L), tumor B (23.2 nmol/L), and tumor C (70.9 nmol/L) was 1.2-, 1.4-, and 4.2-fold of that in the normal brain (16.8 nmol/L), respectively; and the respective $K_{p,uu}$ was 0.38, 0.42, and 1.30 in tumors A, B, and C as compared to 0.34 in the normal brain (**Fig. 4**). Following one-cycle treatment of neratinib (240 mg once daily, 21 days), the simulated population mean $C_{ss,ave}$ of unbound neratinib in tumor A (1.12 nmol/L), tumor B (3.48 nmol/L), and tumor C (4.22 nmol/L) was 1.6-, 5.1-, and 6.2-fold of that in the normal brain (0.68 nmol/L), respectively; and the corresponding $K_{p,uu}$ was 1.72, 5.34, and 6.52 in tumors A. B, and C as compared to 1.06 in the normal brain (**Fig. 4**).

Target engagement ratio in the human normal brain and brain metastases

Target engagement ratio is defined as the ratio of the average steady-state unbound drug brain concentration to the *in vitro* IC_{50} for HER2 inhibition (36). Theoretically, a target engagement ratio ≥ 1 would lead to 50% or greater inhibition of HER2. The IC_{50} of tucatinib, lapatinib, and neratinib for inhibition of HER2 kinase was determined as 6.9, 109, and 5.6 nmol/L, respectively, by ADP-Glo assay (37). Thus, based on the model-predicted population mean $C_{ss,ave}$ of unbound drug in the human normal brain and hypothesized brain metastasis tumors following 1-cycle of standard dosing, the respective mean HER2 target engagement ratios achieved in the normal brain, tumor A, tumor B, and tumor C were 2.1, 2.4, 5.1, and 5.4 for tucatinib; 0.15, 0.19, 0.21, and 0.65 for lapatinib; and 0.12, 0.20, 0.62, and 0.75 for neratinib.

Discussion

Drug penetration into the human brain is restricted by the BBB, which is composed of a continuous layer of brain microvascular endothelial cells that are connected by tight junctions, covered by a basal membrane and astrocytic perivascular end-feet, and expressed with active transporters and receptors (38–40). Because tight junctions restrict paracellular exchange between the blood and brain, the penetration of most drugs across the BBB is mainly controlled by transcellular passive diffusion and transporter-mediated active transport (41, 42). The physical and biochemical barriers of the BBB in brain metastases are often disrupted albeit to different degree, leading to increased drug penetration into bulky tumors (43–45). However, the BBB remains largely or completely intact in smaller aggregates of metastasized tumor cells (i.e., micrometastases), while these regions are often undetectable or unresectable and cause recurrent disease (43). Therefore, to treat asymptomatic micrometastases or prevent metastatic disease from occurring or recurring, a potentially clinical successful therapeutic agent must penetrate an intact BBB to achieve adequate pharmacologically active (or unbound) drug concentrations for target inhibition.

Target engagement ratio, which is determined by the unbound drug brain/tumor concentration and drug potency for target inhibition, can be used as a pharmacodynamic indicator of intracranial efficacy. In the present study, a target engagement ratio ≥ 1 (theoretically resulting in ≥ 50% target inhibition) achieved in the normal brain is considered as the threshold for sufficient HER2 inhibition in brain metastases including micrometastases behind an intact BBB. Tucatinib, lapatinib, and neratinib are distinct with respect to the physicochemical properties, binding to plasma proteins and brain tissue, passive transcellular permeability, as well as interactions with metabolizing enzymes and transporters (**Table 1** and S1). It is therefore not surprising that the three HER2 inhibitors differ in the plasma and CNS pharmacokinetic profiles in patients (**Fig. 2**). PBPK model simulations suggest that following 1 cycle (21 days) of standard dosing, tucatinib and lapatinib achieve similar unbound drug brain exposure ($C_{ss,ave,br}$, 14.5 vs. 16.8 nmol/L); whereas, the brain exposure of unbound neratinib ($C_{ss,ave,br}$, 0.68 nmol/L) is 20-fold lower due to its extremely low unbound drug plasma exposure (**Table 2**). On the other hand, while sharing similar mechanism of action, the three HER2 inhibitors differ in the specificity and potency for inhibition of ERBB family receptors. Tucatinib and neratinib are equally potent (IC_{50}, 6.9 vs. 5.6 nmol/L) for HER2 inhibition, while lapatinib (IC_{50}, 109 nmol/L) is over 10-fold less potent (37). Taken together, following 1 cycle of standard dosing, tucatinib achieves HER2 target engagement ratio of 2.1 in a typical patient's brain or micrometastases behind an intact BBB; whereas, the target engagement ratio is less than 0.20 for lapatinib (due to weak potency) and neratinib (due to low unbound drug brain exposure). In brain metastasis tumors with a disrupted BBB and relatively acidic tumor microenvironment, the target engagement ratio increases because of enhanced drug tumor penetration (**Fig. 4**). For example, in the hypothesized tumor C (i.e., with tumor pH 6.5, loss of ABCB1 and ABCG2 expression at the BBB, and leaky tight junctions leading to 5-fold increase of passive permeability), the target engagement ratios of tucatinib, lapatinib, and neratinib increase to 5.4, 0.58, and 0.75, respectively, following 1 cycle of standard dosing. Therefore, based on the target engagement ratio, tucatinib appears to be the most efficacious among the three HER2 kinase inhibitors for the treatment brain metastases (including micrometastases) in patients with HER2-positive breast cancer. By contrast, the intracranial efficacy of lapatinib and neratinib remain elusive due to insufficient target inhibition (i.e., target engagement ratios < 1.0) even in metastatic tumors with a disrupted BBB. These data provide important pharmacologic insights into the observed clinical efficacy data of these drugs in HER2-positive breast cancer patients with brain metastases.

Tucatinib, a reversible, highly specific tyrosine kinase inhibitor of HER2, received the FDA approval in 2020 for use in combination with trastuzumab and capecitabine for the treatment of patients with advanced or metastatic HER2-positive breast cancer, including patients with brain metastases, who have received one or more prior anti-HER2 based regimens. A randomized, double-blind, placebo-controlled trial (HER2CLIMB) has provided strong evidence for the intracranial efficacy and overall survival benefit of tucatinib in combination with trastuzumab and capecitabine among heavily pretreated HER2-positive breast cancer patients with active or stable brain metastases (11, 12). Specifically, the addition of tucatinib to trastuzumab and capecitabine doubled intracranial objective response rate (47.3% vs. 20.0%, $P = 0.03$), reduced risk of intracranial progression or

death by two thirds [HR, 0.32; 95% confidence interval (CI), 0.22–0.48; $P < 0.0001$], and reduced risk of death by nearly half (HR, 0.58; 95% CI, 0.40–0.85; $P = 0.005$; ref. 12). Recently reported data on the additional 15.6 months of follow-up in HER2CLIMB trial suggested that the tucatinib plus trastuzumab and capecitabine regimen resulted in a robust and durable prolongation of overall survival for all patients with HER2-positive metastatic breast cancer and brain metastases, and this benefit was maintained in patients with untreated or treated progressing brain metastases as well as treated stable brain metastases (46). Notably, the significant and clinically meaningful intracranial efficacy and overall survival benefit of tucatinib observed in patients with active or stable brain metastases is consistent with and supported by PBPK model prediction indicating that tucatinib achieves sufficient HER2 inhibition (with target engagement ratio > 2.0) in not only brain metastases with a disrupted BBB but also micrometastases behind an intact BBB.

Lapatinib, a reversible, dual tyrosine kinase inhibitor of HER2 and EGFR, is the first FDA-approved small-molecule HER2 inhibitor for use in combination with capecitabine for the treatment of metastatic HER2-positive breast cancer. Lapatinib monotherapy showed marginal intracranial activity with a CNS objective response rate of 2.6% to 6% in pretreated HER2-positive breast cancer patients with progressive brain metastases (8, 47). The combination of lapatinib and capecitabine increased the CNS response rate to 66% among previously untreated HER2-positive breast cancer patients with brain metastases (48). The CNS response rate was further enhanced when lapatinib was combined with whole-brain radiation therapy (79%) or stereotactic radiosurgery (75%; refs. 49, 50). Of note, the CNS response rate in the combination therapies should be interpreted with caution. Given the clinical observed marginal intracranial activity of lapatinib monotherapy and insufficient target engagement (even in brain metastases with a largely disrupted BBB) as revealed by PBPK modeling, the increased CNS response rate with lapatinib-capecitabine combination was likely due to a better systematic extracranial disease control by the combination therapy. The significantly increased CNS response rate with lapatinib-brain radiation combination could be largely driven by the intracranial efficacy of whole-brain radiation or stereotactic radiosurgery and also partly attributable to better extracranial disease control by lapatinib. Furthermore, a prospective randomized trial (CEREBEL) indicated no difference between lapatinib-capecitabine and trastuzumab-capecitabine regimens with respect to the rate of CNS disease progression in metastatic HER2-positive breast cancer patients with asymptomatic brain metastases at entry, suggesting the intracranial activity of lapatinib is not superior to trastuzumab, a humanized monoclonal anti-HER2 antibody that is known to poorly penetrate the BBB and have mild (if any) intracranial activity (5). Collectively, these clinical data, supported by insufficient target inhibition as revealed by the PBPK modeling, suggest that lapatinib would be unlikely to exert significant and clinically meaningful intracranial efficacy among patients with active or stable brain metastases.

Different from tucatinib and lapatinib, neratinib is an irreversible pan-HER (HER1, HER2, and HER4) tyrosine kinase inhibitor. It received FDA approval in 2017 for the extended adjuvant treatment of patients with early-stage HER2-positive breast cancer, and then in 2020 for use in combination with capecitabine for patients with advanced or metastatic HER2-positive breast cancer. Neratinib monotherapy demonstrated a similar intracranial activity as lapatinib, with a CNS objective response rate of 8% (versus 6% for lapatinib) in pretreated HER2-positive breast cancer patients with progressive CNS disease (47, 51). In addition, the clinical efficacy of neratinib plus capecitabine was compared to lapatinib plus capecitabine in heavily pretreated HER2-positive metastatic breast cancer patients in a randomized phase III trial (NALA; ref. 10). Neratinib plus capecitabine showed a statistically significant benefit in progression-free survival but not in overall survival; and notably, fewer patients in neratinib plus capecitabine arm required intervention for CNS metastases than those in lapatinib plus capecitabine arm, but the difference was modest (cumulative incidence of intervention, 22.8% vs. 29.2%; $P = 0.043$; ref. 10). Furthermore, the clinical efficacy of neratinib plus paclitaxel was compared to trastuzumab plus paclitaxel in patients with previously untreated metastatic HER2-positive breast cancer in a randomized, controlled, open-label trial (NEfERT-T; ref. 9). Although neratinib plus paclitaxel significantly delayed the time to CNS metastases (hazard ratio 0.45; 95% CI 0.26–0.78; $P = 0.004$) and reduced the incidence of symptomatic or progressive CNS recurrence (8.3% vs. 17.3%), the seemingly better intracranial disease control was not translated to a better overall survival or progression-free survival (9). Collectively, neratinib appears to have slightly or modestly better intracranial activity than lapatinib or trastuzumab in patients with metastatic HER2-positive breast cancer. However, a clinically relevant intracranial efficacy that can be translated to the long-term efficacy (i.e., overall survival benefit) has not been demonstrated. These clinical data are consistent with the PBPK model prediction that neratinib achieves slightly better target engagement ratios in metastatic tumors (with the disrupted BBB and relatively acidic tumor pH) than lapatinib (e.g., 0.62 vs. 0.21 in tumor B; 0.75 vs. 0.65 in tumor C); whereas, in the brain or micrometastasis tumors behind an intact BBB, both drugs show similar target ratios (0.12 vs. 0.15; which are significantly lower than the threshold ratio of 1.0 for adequate HER2 inhibition). Therefore, similar to lapatinib, neratinib would be unlikely effective to treat asymptomatic micrometastases or prevent metastatic disease from occurring or recurring. This could explain, at least in part, for the lack of long-term efficacy (i.e., overall survival benefit) as compared to lapatinib or trastuzumab in patients with metastatic HER2-positive breast cancer. The inability of neratinib for prevention of brain metastases has been further confirmed in a large randomized, double-blind, placebo-controlled Phase III trial (ExteNET), whereby patients with early-stage HER2-positive breast cancer received a 1-year treatment of either neratinib (240 mg, once daily; $n = 1{,}420$) or placebo ($n = 1{,}420$) within 1–2 years of completing standard trastuzumab-based therapy (52). Although neratinib significantly improved disease-free survival as compared with placebo (HR, 0.63; 95% CI, 0.46–0.84; $P = 0.0017$), cumulative incidence of CNS metastases showed no statistically significant difference between two groups (52).

In conclusion, as revealed by the PBPK model simulations, tucatinib induces sufficient HER2 inhibition (with the population mean target engagement ratio > 2.0) in not only bulky brain metastasis tumors with a disrupted BBB, but also in micrometastases where the BBB largely remains intact. By contrary, lapatinib and neratinib may not achieve sufficient target (HER2) inhibition (with the population mean target engagement ratio < 1.0) even in tumors with disrupted BBB and relatively acidic tumor microenvironment. These findings, in line with available clinical pharmacokinetic and efficacy data, support the therapeutic value of tucatinib for the treatment of brain metastatasis in patients with HER2-positive breast cancer. In addition, given its capability of penetrating an intact BBB to achieve adequate target engagement, further clinical investigation of tucatinib for the prevention of brain metastases in patients with HER2-positive breast cancer is warranted.

Authors' Disclosures

J. Li reports grants from Seagen Inc. and grants from NIH/NCI during the conduct of the study. V. Kumar reports other support from Seagen Inc. outside the submitted work. S.C. Alley is an employee and stockholder of Seagen Inc. S. Peterson reports other support from Seagen Inc. outside the submitted work; in addition, S. Peterson has a patent for US11207324B2 issued to Seagen Inc. A.J. Lee reports other support from Seagen Inc. outside the submitted work; in addition, A.J. Lee has a patent for 62/797,854 pending. No disclosures were reported by the other authors.

Authors' Contributions

J. Li: Conceptualization, formal analysis, supervision, funding acquisition, validation, investigation, methodology, writing–original draft, project administration, writing–review and editing. **J. Jiang:** Validation, investigation, methodology, writing–review and editing. **X. Bao:** Methodology. **V. Kumar:** Data curation, writing–review and editing. **S.C. Alley:** Data curation, writing–review and editing. **S. Peterson:** Data curation, writing–review and editing. **A.J. Lee:** Conceptualization, data curation, project administration, writing–review and editing.

Acknowledgments

This study was supported, in part, by the NIH Cancer Center Support Grant P30 CA022453 and Seagen Inc.

The publication costs of this article were defrayed in part by the payment of publication fees. Therefore, and solely to indicate this fact, this article is hereby marked "advertisement" in accordance with 18 USC section 1734.

Note

Supplementary data for this article are available at Clinical Cancer Research Online (http://clincancerres.aacrjournals.org/).

Received February 6, 2022; revised March 24, 2022; accepted May 12, 2022; published first May 18, 2022.

References

1. Cronin KA, Harlan LC, Dodd KW, Abrams JS, Ballard-Barbash R. Population-based estimate of the prevalence of HER-2 positive breast cancer tumors for early stage patients in the US. Cancer Invest 2010;28:963–8.
2. Brufsky AM, Mayer M, Rugo HS, Kaufman PA, Tan-Chiu E, Tripathy D, et al. Central nervous system metastases in patients with HER2-positive metastatic breast cancer: incidence, treatment, and survival in patients from registHER. Clin Cancer Res 2011;17:4834–43.
3. Leyland-Jones B. Human epidermal growth factor receptor 2-positive breast cancer and central nervous system metastases. J Clin Oncol 2009; 27:5278–86.
4. Pestalozzi BC, Brignoli S. Trastuzumab in CSF. J Clin Oncol 2000;18:2349–51.
5. Seligmann JF, Wright-Hughes A, Pottinger A, Velikova G, Oughton JB, Murden G, et al. Lapatinib plus capecitabine versus trastuzumab plus capecitabine in the treatment of human epidermal growth factor receptor 2-positive metastatic breast cancer with central nervous system metastases for patients currently or previously treated with trastuzumab (LANTERN): a phase II randomised trial. Clin Oncol (R Coll Radiol) 2020;32:656–64.
6. Freedman RA, Gelman RS, Anders CK, Melisko ME, Parsons HA, Cropp AM, et al. TBCRC 022: a phase II trial of neratinib and capecitabine for patients with human epidermal growth factor receptor 2-positive breast cancer and brain metastases. J Clin Oncol 2019;37:1081–9.
7. Yardley DA, Hart LL, Ward PJ, Wright GL, Shastry M, Finney L, et al. Cabazitaxel plus lapatinib as therapy for HER2(+) metastatic breast cancer with intracranial metastases: results of a dose-finding study. Clin Breast Cancer 2018;18:e781–e7.
8. Lin NU, Carey LA, Liu MC, Younger J, Come SE, Ewend M, et al. Phase II trial of lapatinib for brain metastases in patients with human epidermal growth factor receptor 2-positive breast cancer. J Clin Oncol 2008;26: 1993–9.
9. Awada A, Colomer R, Inoue K, Bondarenko I, Badwe RA, Demetriou G, et al. Neratinib plus paclitaxel vs trastuzumab plus paclitaxel in previously untreated metastatic ERBB2-positive breast cancer: the NEfERT-T randomized clinical trial. JAMA Oncol 2016;2:1557–64.
10. Saura C, Oliveira M, Feng YH, Dai MS, Chen SW, Hurvitz SA, et al. Neratinib plus capecitabine versus lapatinib plus capecitabine in HER2-positive metastatic breast cancer previously treated with >/= 2 HER2-directed regimens: phase III NALA trial. J Clin Oncol 2020;38:3138–49.
11. Lin NU, Borges V, Anders C, Murthy RK, Paplomata E, Hamilton E, et al. Intracranial efficacy and survival with tucatinib plus trastuzumab and capecitabine for previously treated HER2-positive breast cancer with brain metastases in the HER2CLIMB trial. J Clin Oncol 2020;38:2610–9.
12. Murthy RK, Loi S, Okines A, Paplomata E, Hamilton E, Hurvitz SA, et al. Tucatinib, trastuzumab, and capecitabine for HER2-positive metastatic breast cancer. N Engl J Med 2020;382:597–609.
13. Deo AK, Theil FP, Nicolas JM. Confounding parameters in preclinical assessment of blood-brain barrier permeation: an overview with emphasis on species differences and effect of disease states. Mol Pharm 2013;10:1581–95.
14. Jamei M, Dickinson GL, Rostami-Hodjegan A. A framework for assessing inter-individual variability in pharmacokinetics using virtual human populations and integrating general knowledge of physical chemistry, biology, anatomy, physiology and genetics: A tale of 'bottom-up' vs 'top-down' recognition of covariates. Drug Metab Pharmacokinet 2009;24:53–75.
15. Zhao P, Zhang L, Grillo JA, Liu Q, Bullock JM, Moon YJ, et al. Applications of physiologically based pharmacokinetic (PBPK) modeling and simulation during regulatory review. Clin Pharmacol Ther 2011;89:259–67.
16. Li J, Zhao M, He P, Hidalgo M, Baker SD. Differential metabolism of gefitinib and erlotinib by human cytochrome P450 enzymes. Clin Cancer Res 2007;13:3731–7.
17. Bao X, Wu J, Sanai N, Li J. Determination of total and unbound ribociclib in human plasma and brain tumor tissues using liquid chromatography coupled with tandem mass spectrometry. J Pharm Biomed Anal 2019;166:197–204.
18. Li J, Wu J, Bao X, Honea N, Xie Y, Kim S, et al. Quantitative and mechanistic understanding of AZD1775 penetration across human blood-brain barrier in glioblastoma patients using an IVIVE-PBPK modeling approach. Clin Cancer Res 2017;23:7454–66.
19. Li J, Kim S, Sha X, Wiegand R, Wu J, LoRusso P. Complex disease-, gene-, and drug-drug interactions: impacts of renal function, CYP2D6 phenotype, and OCT2 activity on veliparib pharmacokinetics. Clin Cancer Res 2014;20:3931–44.
20. Bao X, Wu J, Jiang J, Tien AC, Sanai N, Li J. Quantitative protein expression of blood-brain barrier transporters in the vasculature of brain metastases of patients with lung and breast cancer. Clin Transl Sci 2021;14:1265–71.
21. Gaohua L, Neuhoff S, Johnson TN, Rostami-Hodjegan A, Jamei M. Development of a permeability-limited model of the human brain and cerebrospinal fluid (CSF) to integrate known physiological and biological knowledge: Estimating time varying CSF drug concentrations and their variability using in vitro data. Drug Metab Pharmacokinet 2016;31:224–33.
22. Kalvass JC, Pollack GM. Kinetic considerations for the quantitative assessment of efflux activity and inhibition: implications for understanding and predicting the effects of efflux inhibition. Pharm Res 2007;24:265–76.
23. Li J, Jiang J, Wu J, Bao X, Sanai N. Physiologically based pharmacokinetic modeling of central nervous system pharmacokinetics of CDK4/6 inhibitors to guide selection of drug and dosing regimen for brain cancer treatment. Clin Pharmacol Ther 2021;109:494–506.
24. Stringer-Reasor EM, O'Brien BJ, Topletz-Erickson A, White JB, RK M. Pharmacokinetic (PK) analyses in CSF and plasma from TBCRC049, an ongoing trial to assess the safety and efficacy of the combination of tucatinib, trastuzumab and capecitabine for the treatment of leptomeningeal metastasis (LM) in HER2 positive breast cancer. J Clin Oncol 39:15s, 2021 (suppl; abstr 1044).
25. Lee A, Jiang J, Kumar V, Alley S, Peterson S, Li J. Physiologically based pharmacokinetic (PBPK) modeling of the central nervous system (CNS) pharmacokinetics of tucatinib in patients with breast cancer brain metastasis. Ann Oncol 2020;31(Suppl 4):S360.
26. Morikawa A, Peereboom DM, Thorsheim HR, Samala R, Balyan R, Murphy CG, et al. Capecitabine and lapatinib uptake in surgically resected brain metastases from metastatic breast cancer patients: a prospective study. Neuro Oncol 2015; 17:289–95.
27. Gori S, Lunardi G, Inno A, Foglietta J, Cardinali B, Del Mastro L, et al. Lapatinib concentration in cerebrospinal fluid in two patients with HER2-positive metastatic breast cancer and brain metastases. Ann Oncol 2014;25:912–3.
28. Freedman RA, Gelman RS, Agar NYR, Santagata S, Randall EC., Gimenez-Cassina Lopez B, et al. Pre- and postoperative neratinib for HER2-positive breast

cancer brain metastases: translational breast cancer research consortium 022. Clin Breast Cancer 2020;20:145–51.
29. Redzic Z. Molecular biology of the blood-brain and the blood-cerebrospinal fluid barriers: similarities and differences. Fluids Barriers CNS 2011;8:3.
30. Daood M, Tsai C, Ahdab-Barmada M, Watchko JF. ABC transporter (P-gp/ABCB1, MRP1/ABCC1, BCRP/ABCG2) expression in the developing human CNS. Neuropediatrics 2008;39:211–8.
31. Rao VV, Dahlheimer JL, Bardgett ME, Snyder AZ, Finch RA, Sartorelli AC, et al. Choroid plexus epithelial expression of MDR1 P glycoprotein and multidrug resistance-associated protein contribute to the blood-cerebrospinal-fluid drug-permeability barrier. Proc Natl Acad Sci U S A 1999;96:3900–5.
32. Bao X, Wu J, Xie Y, Kim S, Michelhaugh S, Jiang J, et al. Protein expression and functional relevance of efflux and uptake drug transporters at the blood-brain barrier of human brain and glioblastoma. Clin Pharmacol Ther 2020;107:1116–27.
33. Honasoge A, Sontheimer H. Involvement of tumor acidification in brain cancer pathophysiology. Front Physiol 2013;4:316.
34. Zhang X, Lin Y, Gillies RJ. Tumor pH and its measurement. J Nucl Med 2010;51:1167–70.
35. Casey JR, Grinstein S, Orlowski J. Sensors and regulators of intracellular pH. Nat Rev Mol Cell Biol 2010;11:50–61.
36. Raub TJ, Wishart GN, Kulanthaivel P, Staton BA, Ajamie RT, Sawada GA, et al. Brain exposure of two selective dual CDK4 and CDK6 inhibitors and the antitumor activity of CDK4 and CDK6 inhibition in combination with temozolomide in an intracranial glioblastoma xenograft. Drug Metab Dispos 2015;43:1360–71.
37. Kulukian A, Lee P, Taylor J, Rosler R, de Vries P, Watson D, et al. Preclinical activity of HER2-selective tyrosine kinase inhibitor tucatinib as a single agent or in combination with trastuzumab or docetaxel in solid tumor models. Mol Cancer Ther 2020;19:976–87.
38. Henderson JT, Piquette-Miller M. Blood-brain barrier: an impediment to neuropharmaceuticals. Clin Pharmacol Ther 2015;97:308–13.
39. Pardridge WM. Drug transport across the blood-brain barrier. J Cereb Blood Flow Metab 2012;32:1959–72.
40. van Tellingen O, Yetkin-Arik B, de Gooijer MC, Wesseling P, Wurdinger T, de Vries HE. Overcoming the blood-brain tumor barrier for effective glioblastoma treatment. Drug Resist Updat 2015;19:1–12.
41. Loscher W, Potschka H. Blood-brain barrier active efflux transporters: ATP-binding cassette gene family. NeuroRx 2005;2:86–98.
42. Miller DS. Regulation of ABC transporters at the blood-brain barrier. Clin Pharmacol Ther 2015;97:395–403.
43. Arvanitis CD, Ferraro GB, Jain RK. The blood-brain barrier and blood-tumour barrier in brain tumours and metastases. Nat Rev Cancer 2020;20:26–41.
44. Gerstner ER, Fine RL. Increased permeability of the blood-brain barrier to chemotherapy in metastatic brain tumors: establishing a treatment paradigm. J Clin Oncol 2007;25:2306–12.
45. van den Bent MJ. The role of chemotherapy in brain metastases. Eur J Cancer 2003;39:2114–20.
46. Lin NU, Murthy RK, Abramson V, Anders C, Bachelot T, Bedard P, et al. Updated results of tucatinib vs placebo added to trastuzumab and capecitabine for patients with previously treated HER2-positive metastatic breast cancer with brain metastases (HER2CLIMB) [abstract]. In: Proceedings of the 2021 San Antonio Breast Cancer Symposium; 2021 Dec 7–10; San Antonio, TX. Philadelphia (PA): AACR; 2022. Abstract nr PD4-04.
47. Lin NU, Dieras V, Paul D, Lossignol D, Christodoulou C, Stemmler HJ, et al. Multicenter phase II study of lapatinib in patients with brain metastases from HER2-positive breast cancer. Clin Cancer Res 2009;15:1452–9.
48. Bachelot T, Romieu G, Campone M, Dieras V, Cropet C, Dalenc F, et al. Lapatinib plus capecitabine in patients with previously untreated brain metastases from HER2-positive metastatic breast cancer (LANDSCAPE): a single-group phase 2 study. Lancet Oncol 2013;14:64–71.
49. Lin NU, Freedman RA, Ramakrishna N, Younger J, Storniolo AM, Bellon JR, et al. A phase I study of lapatinib with whole brain radiotherapy in patients with human epidermal growth factor receptor 2 (HER2)-positive breast cancer brain metastases. Breast Cancer Res Treat 2013;142:405–14.
50. Kim JM, Miller JA, Kotecha R, Chao ST, Ahluwalia MS, Peereboom DM, et al. Stereotactic radiosurgery with concurrent HER2-directed therapy is associated with improved objective response for breast cancer brain metastasis. Neuro Oncol 2019;21:659–68.
51. Freedman RA, Gelman RS, Wefel JS, Melisko ME, Hess KR, Connolly RM, et al. Translational breast cancer research consortium (TBCRC) 022: a phase II trial of neratinib for patients with human epidermal growth factor receptor 2-positive breast cancer and brain metastases. J Clin Oncol 2016;34:945–52.
52. Martin M, Holmes FA, Ejlertsen B, Delaloge S, Moy B, Iwata H, et al. Neratinib after trastuzumab-based adjuvant therapy in HER2-positive breast cancer (ExteNET): 5-year analysis of a randomised, double-blind, placebo-controlled, phase 3 trial. Lancet Oncol 2017;18:1688–700.